Journal of Materials Chemistry A

A minimal non-radiative recombination loss for efficient non-fullerene all-small-molecules organic solar cells with low energy loss of 0.54 eV and high open-circuit voltage of 1.15 V

Journal:	*Journal of Materials Chemistry A*
Manuscript ID	TA-ART-05-2018-004665.R1
Article Type:	Paper
Date Submitted by the Author:	23-Jun-2018
Complete List of Authors:	Yang, Daobin; Yamagata Daigaku Kogakubu Daigakuin Rikogaku Kenkyuka, Department of Organic Device Engineering, Research Center for Organic Electronics Wang, Yuming; Linkoping University, Department of Physics, Chemistry and Biology (IFM) Sano, Takeshi; Yamagata University, Gao, Feng; Linkoping University, Department of Physics, Chemistry and Biology (IFM) Sasabe, Hisahiro; Yamagata univ., Organic Device Engineering Kido, Junji; Yamagata University Faculty of Engineering Graduate School of Science and Engineering

A minimal non-radiative recombination loss for efficient non-fullerene all-small-molecules organic solar cells with low energy loss of 0.54 eV and high open-circuit voltage of 1.15 V

Daobin Yang,[a,b,†] *Yuming Wang,*[c,†] *Takeshi Sano,**[a,b,d] *Feng Gao,**[c] *Hisahiro Sasabe,**[a,b,d] *and Junji Kido* [a,b,d]

[a] *Research Center for Organic Electronics (ROEL), Yamagata University, Yonezawa 992-8510, Japan*

[b] *Frontier Center for Organic Materials (FROM), Yamagata University, Yonezawa 992-8510, Japan*

[c] *Department of Physics Chemistry and Biology (IFM), Linköping University, Linköping SE-58183, Sweden*

[d] *Department of Organic Materials Science, Yamagata University, Yonezawa 992-8510, Japan*

* *E-mail: takeshi.sano@yz.yamagata-u.ac.jp; feng.gao@liu.se*; *h-sasabe@yz.yamagata-u.ac.jp*

† *D. Yang and Y. Wang contributed equally to this work.*

Keywords: low energy loss, high open-circuit voltage, non-radiative recombination, non-fullerene, all-small-molecules organic solar cells

Abstract: Organic solar cells (OSCs) are considered as a promising next-generation photovoltaic technology because of their light weight, flexibility, and the potential of roll-to-roll fabrication. However, the relatively large energy loss (E_{loss}) from the optical bandgap (E_g) of the absorber to the open-circuit voltage (V_{oc}) of the device hinders further improvement of the PCEs of OSCs. Here, we report efficient non-fullerene all-small-molecules

organic solar cells (NF all-SMOSCs), using DR3TBDTT and O-IDTBR as donor and acceptor, respectively. We obtain a high electroluminescence yield (EQE_{EL}) value of up to of ~4 ×10^{-4} corresponding to a 0.21 eV non-radiative recombination energy loss, which is the smallest value for bulk-heterojunction (BHJ) OSCs so far. As a result, a low E_{loss} of 0.54 eV and a considerably high V_{oc} of 1.15 V are obtained for BHJ NF all-SMOSCs.

1. Introduction

Bulk heterojunction (BHJ) organic solar cells (OSCs) are considered as a very promising clean energy technology because of their light weight, flexibility, and the potential of roll-to-roll fabrication. [1,2] After the great efforts on the new materials design and synthesis [3-6] and the devices optimization, [7-9] the current record highest power conversion efficiency (PCE) of single-junction BHJ-OSCs is achieved over 13%. [10-12] However, the PCEs of BHJ-OSCs still significantly lower than those of inorganic solar cells and perovskite solar cells (over 20%). [13,14] One of the most important reasons that limits the PCEs of OSCs is the relatively large energy loss (E_{loss}) from the optical bandgap (E_g) of the absorber to the open-circuit voltage (V_{oc}) of the device, which is defined as E_{loss}= $E_g - qV$oc. [15-18] The E_{loss} of inorganic crystalline and perovskite solar cells are normally between 0.30 and 0.55 eV. [19,20] In contrast, the E_{loss} for fullerene-based OSCs with high PCEs is often observed between 0.6 and 1.0 eV. [21-23] Such large E_{loss} in OSCs can be ascribed to two main reasons. One reason is the non-steep absorption onset due to the charge transfer (CT) within the band gap. [20] Another is the large non-radiative recombination losses (typically, between 0.35 and 0.44 eV), identified by the very low electroluminescence yields (EQE_{EL}), usually between 10^{-6} and 10^{-8}. [24,25] The

non-radiative recombination losses often constitute a significant part of the total energy losses in BHJ-OSCs. Therefore, the most effective strategy to reduce the energy loss is to decrease the non-radiative recombination losses, which can improve the EQE_{EL} of OSCs.

Very recently, a few reports show that the E_{loss} for non-fullerene (NF)-based polymer solar cells (PSCs) could reduce to 0.4~0.6 eV with PCEs of over 10%, [22,26-29] indicating that NF-solar cells can be an effective way for achieving low E_{loss}. Furthermore, non-fullerene acceptors present good light harvesting capability, finely tuned energy levels, and facile synthesis, which are beneficial to achieving high open-circuit voltage (V_{oc}) and short-circuit current density (J_{sc}). [30-32] In comparison with the polymeric counterparts, non-fullerene all-small-molecules OSCs (NF all-SMOSCs) should be more promising owing to their well-defined molecular structures, accurate molecular weights, and high purities without batch to batch variations. [33-36] As we know, there are four reports show that the PCEs of single-junction NF all-SMOSCs exceed 9% up to date. [37-40] However, all of their V_{oc} are less than 1.0 V, which are ascribed to the relative large E_{loss} of 0.64~0.72 eV. Therefore, it is essential to develop the OSCs with a low E_{loss} and high V_{oc}, to further enhance the PCEs of OSCs.

In this work, we report efficient NF BHJ all-SMOSCs based on DR3TBDTT (donor) and O-IDTBR (acceptor) (**Fig. 1**). This device shows a high EQE_{EL} of up to ~4×10^{-4} corresponding to ~0.21 eV non-radiative recombination energy loss, which is, to the best of our knowledge, the smallest value as reported in all BHJ-OSCs. Moreover, characterization of Fourier-transform photocurrent spectroscopy external quantum efficiency (FTPS-EQE) spectrum clearly demonstrates that this device has a low additional radiative recombination loss. Consequently, a low E_{loss} of 0.54 eV and a considerably high V_{oc} of 1.15 V are achieved for

BHJ NF all-SMOSCs, which is the first report for SMOSCs. In addition, after optimizing morphology active layers by solvent vapor annealing (SVA), the PCE of the device is improved from 4.30% to 6.36%.

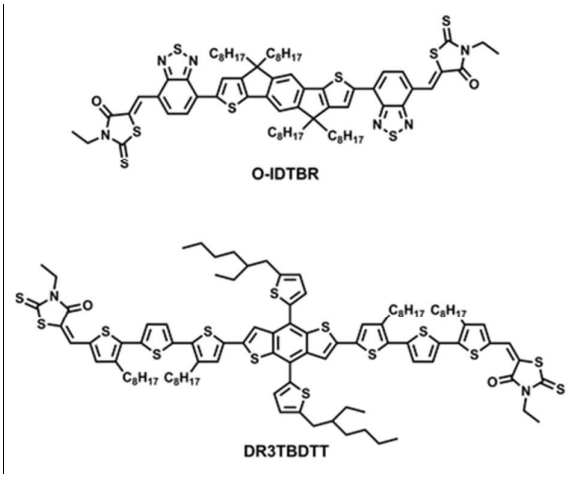

Fig. 1. Chemical structures of the donor and acceptor.

2. Experimental Section

Electron donor DR3TBDTT and electron acceptor O-IDTBR were purchased from Solarmer Materials Inc. Organic solar cells were fabricated using indium-tin-oxide (ITO) coated glass as substrate with the sheet resistance of 10 Ω sq^{-1}. Patterned ITO-coated glass substrates were sequentially cleaned using detergent, deionized water, acetone, and isopropanol in an ultrasonic bath for 30 min each. The cleaned substrates were dried in an oven at 65 ℃ for 12 h before use. The substrates were treated by UV-ozone for 20 min. PEDOT:PSS (Clevios P VP AI 4083, filtered at 0.45μm with PVDF) was spin-coated at 4000 rpm for 40 s on to the ITO surface, and the substrates were heated at 150 ℃ for 20 min before being moved into the glovebox.

Subsequently, the photoactive layers were fabricated by spin-coating a blend of DR3TBDTT: O-IDTBR (0.8: 1, weight ratio) in chloroform with total concentration of 16 mg mL^{-1} in a N_2-filling glovebox at 45 °C for 3 h. The thickness of the photoactive layers is around 90 nm, which is measured by Programmable Surface Profiler Measuring System. Then, these substrates were placed in a glass Petri dish containing 1.5 mL dichloromethane for solvent vapor annealing. Afterwards, the substrates were transferred back to the high-vacuum chamber, where BCP (10 nm) and Al (100 nm) were deposited through a shadow mask by thermal evaporation at pressures of less than 6×10^{-5} Pa with a rate of 0.20 Å s^{-1} and 2×10^{-4} Pa with a rate of 1.5~5.0 Å s^{-1}, respectively, resulting in a final OSCs with the structure of ITO/PEDOT:PSS (40 nm)/DR3TBDTT: O-IDTBR (90 nm)/BCP (10 nm)/Al (100 nm). The active area of organic solar cells is 9 mm^2. Current density-voltage (*J-V*) and external quantum efficiency (EQE) characterizations were performed on a CEP-2000 integrated system manufactured by Bunkoukeiki Co. under 100 mW cm^{-2} simulated AM 1.5G light illumination. All of the measurements were carried out in ambient air.

3. Results and Discussion

3.1 Material Properties

As shown in **Fig. 2a**, UV-Vis absorption spectrum of DR3TBDTT film exhibits a strong and broad absorption at the region of 400-700 nm with a maximum absorption peak of 590 nm, complementary to that of the O-IDTBR film from 500 to 770 nm with a maximum absorption peak of 690 nm, which is beneficial to utilize the visible region of the sunlight. The absorption

edges of DR3TBDTT and O-IDTBR at 720 and 765 nm correspond to the optical bandgap of 1.72 and 1.62 eV, respectively, which are consistent with the previous literatures. [41,42] Meanwhile, as shown in **Fig. 2b**, both the HOMO and LUMO energy levels of O-IDTBR are obviously lower than those of DR3TBDTT (**Fig. S1** and **Table S1**), which can afford a sufficient driving force for exciton dissociation. [44] Therefore, the combination of the two small molecular materials is very suitable for fabricating OSCs.

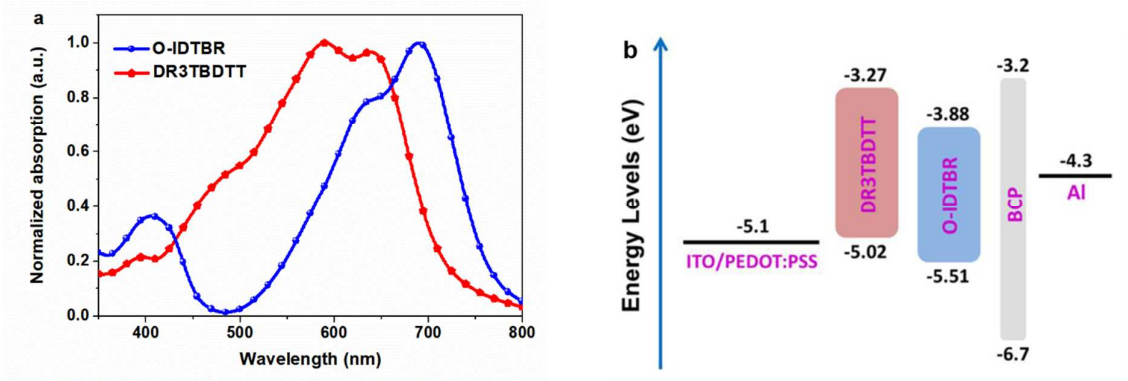

Fig. 2. a) Normalized UV-Vis absorption spectra of the pure donor and acceptor films; b) Schematic energy levels diagrams of materials used in photovoltaic devices. [43]

3.2 Photovoltaic Properties

To study their photovoltaic properties, NF all-SMOSCs devices are fabricated with a normal structure of ITO/ PEDOT:PSS/ DR3TBDTT:O-IDTBR/ BCP/ Al. Chloroform is used as the solvent, and the blend films are optimized by carefully varying the weight ratio of donor and acceptor (*i.e.* D/A, weight ratio), and by adjusting their thickness, their photovoltaic performances are summarized in **Table S2** and **Table S3**, and the corresponding current density-voltage (*J-V*) curves are shown in **Fig. S2** and **Fig. S3**. The photovoltaic performances

of the devices with the optimal D/A blend ratio (0.8:1) and thickness (~90 nm) are further improved by adopting dichloromethane (DCM) as the solvent for solvent vapor annealing (SVA) treatment. The photovoltaic parameters of the devices with different SVA treatment times (40 s, 70 s and 100 s) are summarized in **Table 1**, and the corresponding *J-V* curves are shown in **Fig. 3a**. The as-cast device exhibits a PCE of 4.30%, it is obviously enhanced to 5.15% by 40 s of SVA treatment. By being treatment for 70 s, the PCE was further increased to 6.36% with V_{oc} of 1.15 V, J_{sc} of 11.06 mA cm^{-2}, and FF of 0.50, which is one of the highest values in BHJ NF all-SMOSCs. When the SVA time is further increased to 100 s, the FF value is slightly improved, however, the V_{oc} and J_{sc} values are notably reduced, thereby resulting in a low PCE. Compared to the as-cast device, the distinctly enhanced PCE of the SVA treated devices is mainly attributed to their higher J_{sc} and FF.

The external quantum efficiency (EQE) spectra of the corresponding devices are measured, and they are shown in **Fig. 3b**. The J_{sc}^{EQE} values calculated from the integration of the EQE spectra agree well with the J_{sc} values obtained from the *J-V* curves, only with a 1-3% mismatch. The broad and efficient EQE spectra from 300 to 770 nm indicates that both the DR3TBDTT and O-IDTBR make contribution to the photo-current. Uniform increases of the whole spectral response are clearly observed for the devices with various SVA treatment times. In particular, the device with SVA treatment for 70 s, the EQE value is significantly enhanced with a maximum value of over 50%, which is rarely observed for OSCs with such low E_{loss}.[22,45]

Table 1. Photovoltaic performances of NF all-SMOSCs.

SVA times	V_{oc} [a)] [V]	J_{sc} [a)] [mA cm^{-2}]	J_{SC}^{EQE} [mA cm^{-2}]	FF [a)]	PCE [a)] [%]
as-cast	1.16	8.63	8.48	0.43	4.30
	(1.16 ± 0.01)	(8.52 ± 0.22)		(0.42 ± 0.01)	(4.15 ± 0.15)
40 s	1.15	9.72	9.57	0.46	5.14
	(1.15 ± 0.01)	(9.49 ± 0.37)		(0.46 ± 0.01)	(5.02 ± 0.12)
70 s	1.15	11.06	10.90	0.50	6.36
	(1.15 ± 0.01)	(10.97 ± 0.43)		(0.49 ± 0.01)	(6.18 ± 0.18)
100 s	1.09	9.18	9.42	0.54	5.40
	(1.09 ± 0.01)	(9.13 ± 0.45)		(0.53 ± 0.01)	(5.28 ± 0.12)

[a)] Average values of 16 individual cells together with standard deviations were given in parentheses.

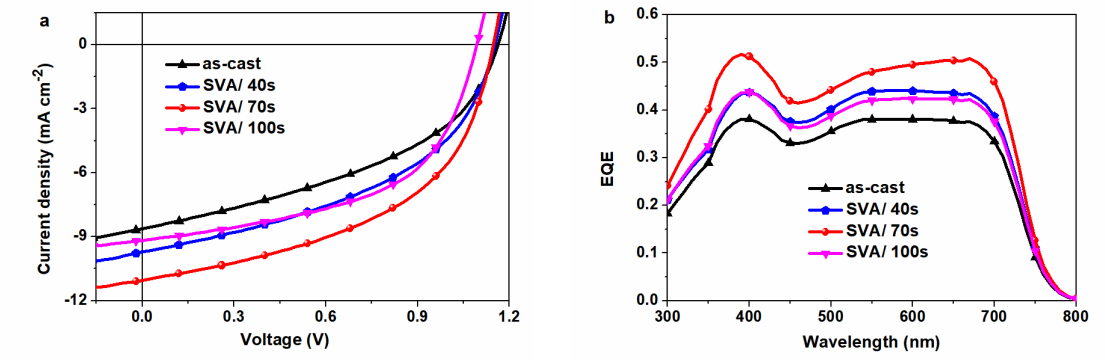

Fig. 3. *J-V* curves (a) and EQE curves (b) of DR3TBDTT: O-IDTBR-based NF all-SMOSCs.

The hole and electron mobilities (μ_h and μ_e) of the DR3TBDTT: O-IDTBR blend films for various SVA treatment times are evaluated using space-charge-limited-current (SCLC) model.

[46] The hole mobility is measured by adopting a hole-only device structure of ITO/MoO_3 /DR3TBDTT:O-IDTBR/MoO_3/Al, and the electron mobility is measured with an electron-only device structure of ITO/ZnO/DR3TBDTT:O-IDTBR/BCP/Al. The μ_h and μ_e values of blend films with various SVA treatment times are summarized in **Table 2**, the corresponding dark *J-V* curves are shown in **Fig. S4**. For the as-cast device, the μ_h is 8.58×10^{-5} cm^2 V^{-1} s^{-1}, which is much lower than its μ_e (1.96×10^{-4} cm^2 V^{-1} s^{-1}), the unbalanced mobility can induce strong charge carrier recombination, resulting in low J_{sc} and FF. After being SVA treatment, both of the μ_h and μ_e of blend films are enhanced, for example, under the optimal condition (SVA for 70 s), the μ_h and μ_e of the blend film reach 2.21×10^{-4} and 3.26×10^{-4} cm^2 V^{-1} s^{-1}, respectively. These high mobilities together with the balanced μ_h/μ_e, resulting in higher charge carrier extraction efficiency, and hence obviously improved J_{sc} and FF could be achieved in this device. [47,48]

Table 2. The hole and electron mobilities of NF all-SMOSCs.

SVA times	μ_h [cm^2 V^{-1} s^{-1}]	μ_e [cm^2 V^{-1} s^{-1}]	μ_e/μ_h
as-cast	8.58×10^{-5}	1.96×10^{-4}	2.28
40 s	1.20×10^{-4}	2.71×10^{-4}	2.26
70 s	2.21×10^{-4}	3.26×10^{-4}	1.48
100 s	1.16×10^{-4}	2.53×10^{-4}	2.18

To further understand the relationship between the evolution of the blend films morphology and the device performances, the surface morphology of the blend films with various SVA

treatment times are investigated by atomic force microscopy (AFM). As shown in **Fig. 4**, a uniform and smooth surface morphology with relatively small root-mean-square (RMS) roughness of 1.16 nm is observed for the as-cast film. After SVA treatment, however, apparent aggregation features are observed with increased RMS values of 1.64, 1.89 and 3.20 nm corresponding to SVA times of 40, 70 and 100 s, respectively. These results indicate that SVA treatment induces the aggregation of DR3TBDTT and O-IDTBR in the blend films, which contributes to efficient exciton dissociation and charge transport. Therefore, significantly enhanced J_{sc} and FF are achieved. Whereas upon SVA treatment for 100 s, the film possesses an excessive nanoscale phase separation with the highest RMS value of 3.20 nm, which may account for the low J_{sc}. In addition, the rough surface could also leads to poor interface contact between the active layer and the hole blocking layer, resulting in low V_{oc}. [49]

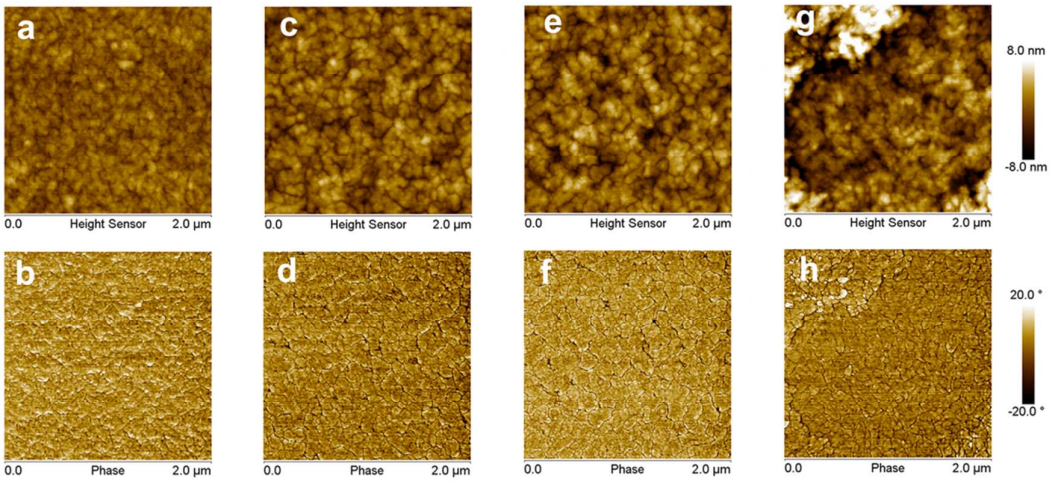

Fig. 4. AFM height and phase images (2×2 µm) of blend films with various SVA treatment times: (a, b) as-cast and after SVA treatment for 40 s (c, d), 70 s (e, f) and 100 s (g, h).

The following grazing-incidence X-ray diffraction (GI-XRD) measurements are performed to provide insight into the crystallinity and molecular orientation of the blend films with

various SVA treatment times. The out of plane and in plane cuts of GI-XRD patterns are given in **Fig. 5** and **Fig. S5**, respectively. In the in-plane direction, no obvious peaks were observed. While all the blend films exhibit the similar peak at 4.50° in the out-of-plane direction, corresponding to a lamellar structure (*d*= 19.6 Å), which come from the pure DR3TBDTT film (**Fig. S6** and **Fig. S7**). These results indicate that the blend films are able to maintain completely edge-on crystalline orientation relative to the substrates. Compared to the as-cast film, stronger diffraction intensities are present in the SVA treated films, and as the treatment times increase, the diffraction intensity improved gradually, indicating a higher degree of molecular ordering. Thus, the high crystalline characteristics of the blend films should promote intermolecular charge transport and reduce charge recombination, eventually resulting in the significantly enhanced J_{sc} and FF in this device.

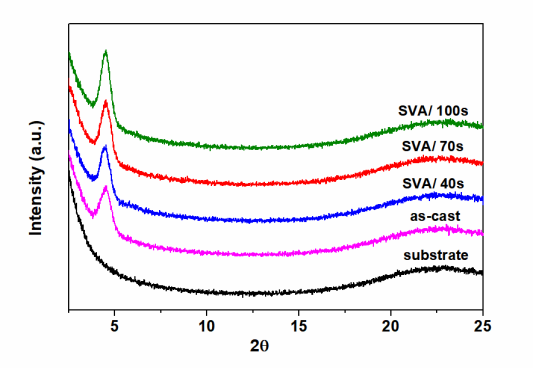

Fig. 5. Out of plane line cuts of the GI-XRD patterns for the blend films with various SVA treatment times.

3.3 Origins of Low Energy Losses

The E_{loss} is determined by the difference between the E_g of the active layer and the V_{oc} of

the device. Most reports employ the onset position of absorption as E_g (1.62 eV in our case), thereby the E_{loss} is as low as 0.48 eV in this device. However, the definition from the absorption onset is not well defined, especially for the films without linear region in the absorption edge or the films with significant light scattering in the absorption tail. In addition to obtaining the E_g from the absorption onset, the E_g can be obtained by taking the crossing point between the absorption and emission spectra of the active layer as well (1.69 eV in our case, **Fig. S8**), corresponding to an E_{loss} of 0.55 eV.

The Shockey-Quessier (SQ) limit and variations thereof is helpful to gaining insight to the energy losses. Based on the SQ limit model, [20,50] the E_{loss} in solar cells can be divided into the three parts as shown in the following equations:

$$E_{loss} = E_g - qV_{oc}$$

$$= (E_g - qV_{\mathrm{oc}}^{\mathrm{SQ}}) + (qV_{\mathrm{oc}}^{\mathrm{SQ}} - qV_{\mathrm{oc}}^{\mathrm{rad}}) + (qV_{\mathrm{oc}}^{\mathrm{rad}} - qV_{oc})$$

$$= \Delta E_1 + \Delta E_2 + \Delta E_3.$$

Where q is the elementary charge, $V_{\mathrm{oc}}^{\mathrm{SQ}}$ is the thermodynamic limit of the V_{oc} in the SQ, $V_{\mathrm{oc}}^{\mathrm{rad}}$ is the radiative limit of V_{oc} where the radiative recombination assumed to be the sole recombination channel in the device. The details for calculating the $V_{\mathrm{oc}}^{\mathrm{SQ}}$ and $V_{\mathrm{oc}}^{\mathrm{rad}}$ are given in ref.50. The quantification results of our NF all-SMOSCs and some other typical solar cells are depicted in **Table 3** and **Fig. 6**.

ΔE_1 is the loss between E_g and $V_{\mathrm{oc}}^{\mathrm{SQ}}$, which is determined by the E_g and temperature. ΔE_2 is the loss between $V_{\mathrm{oc}}^{\mathrm{SQ}}$ and $V_{\mathrm{oc}}^{\mathrm{rad}}$, which is ascribed to non-steep absorption or EQE curve of the real-world devices. OSCs usually have relatively larger ΔE_2, e.g. 0.20 eV for the PTB7: $PC_{71}BM$ blend film-based OSCs, which is due to the CT states within the band gap. As shown in **Fig. S9** and **Fig. S10**, we measured FTPS-EQE and EL spectra for blends and pure acceptor,

and found that no distinct and red-shifted absorption and emission related to CT states are visible in the spectra of blends. As a result, the ΔE_2 is calculated to be as low as 0.06 eV in this device. ΔE_3 is non-radiative recombination energy losses due to the non-radiative recombination at V_{OC} conditions. The ΔE_3 is determined by the EQE_{EL} of the solar cells *i.e.* $\Delta V_3 = \frac{kT}{q}\ln(EQE_{EL})$. For OSCs, this loss is much higher than those of crystalline silicon and perovskite solar cells due to the low EQE_{EL} (usually 10^{-6}~10^{-8}) of CT states. [24] While for P3TEA: SF-PDI_2-based NF-PSCs, this loss can be reduced to 0.26 eV because the EQE_{EL} value is improved to 5×10^{-5}, thereby resulting in a relatively low E_{loss} of 0.61 eV. Remarkably, for the DR3TBDTT: O-IDTBR-based NF all-SMOSCs, a high EQE_{EL} value of 4.0×10^{-4} is observed (**Fig. S11**), even much higher than that of pure film of O-IDTBR (2.4×10^{-6}), which is the highest one in all BHJ-OSCs. It is indicated that this loss is as low as 0.21 eV, even lower than $MAPbI_3$-based perovskite solar cells (0.25 eV). [20] This is, to the best of our knowledge, the smallest non-radiative recombination energy loss in OSCs so far.

Table 3. Comparison between NF all-SMOSCs and other solar cells.

Type of solar cells	Materials	E_g [eV]	qV_{oc} [eV]	E_{loss} [eV]	ΔE_1 [eV]	ΔE_2 [eV]	ΔE_3 [eV]
This work	DR3TBDTT: O-IDTBR	1.69	1.14	0.55	0.28	0.06	0.21
Inorganic	crystalline silicon [a)]	1.12	0.68	0.44	0.25	0.01	0.18
	$MAPbI_3$ [a)]	1.61	1.08	0.53	0.28	0.002	0.25
Polymer	PTB7: $PC_{71}BM$ [a)]	1.61	0.74	0.87	0.28	0.20	0.39
	P3TEA: SF-PDI_2 [b)]	1.72	1.11	0.61	0.27	0.07	0.26

[a)] The original data of energy losses are taken from ref.20.

[b)] The original data of energy losses are taken from ref.50.

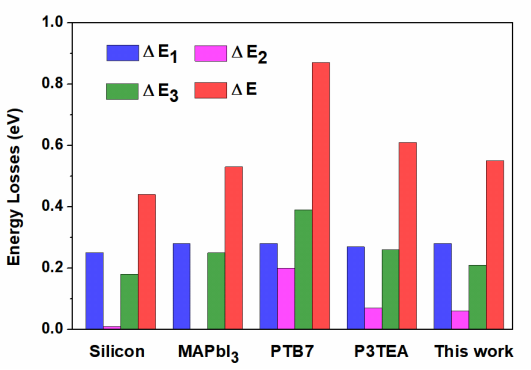

Fig. 6. Histogram of the quantifying energy losses of several inorganic and organic solar cells.

4. Conclusion

In summary, NF BHJ all-SMOSCs are fabricated by using DR3TBDTT and O-IDTBR as donor and acceptor, respectively, showing a minimal non-radiative recombination energy loss of 0.21 eV. Moreover, the steep FTPS-EQE spectrum tail demonstrates that this device has a low additional radiative recombination loss of 0.06 eV. As a result, a low E_{loss} of 0.54 eV with a considerably high V_{oc} of 1.15 V is achieved for BHJ NF all-SMOSCs, which is very close to those of inorganic solar cells and perovskite solar cells. In addition, SVA plays a critical role in the photovoltaic performance in NF all-SMOSCs, which increases the crystallinity of the donor and acceptor, promotes the proper phase separation domain size, and improves charge transport. Consequently, the PCE of the device is enhanced from 4.30% to 6.36%, which is the highest one as reported in SMOSCs with such low E_{loss} and high V_{oc}. This remarkable result exhibits a great potential for the development of NF all-SMOSCs, and creates a path towards efficient OSCs with a low E_{loss}.

Acknowledgements

We acknowledge financial support for this work by the Japan Science and Technology Agency (JST) and Ministry of Education, Culture, Sports, Science and Technology (MEXT) for financial support through the Center of Innovation (COI) Program, and the Swedish Energy Agency Energimyndigheten (2016-010174). We also thank Mr. Yuya Hayashi for the technical assistance of PYS measurement.

References

[1] C. Yan, S. Barlow, Z. Wang, H. Yan, A. K. Y. Jen, S. R. Marder and X. Zhan, *Nat. Rev. Mater.*, 2018, **3**, 18003.

[2] L. Dou, Y. Liu, Z. Hong, G. Li and Y. Yang, *Chem. Rev.*, 2015, **115**, 12633-12665.

[3] J. Du, M. C. Biewer and M. C. Stefan, *J. Mater. Chem. A*, 2016, **4**, 15771-15787.

[4] Y. Lin and X. Zhan, *Acc. Chem. Res.*, 2016, **49**, 175-183.

[5] Q. Zhang, M. A. Kelly, N. Bauer and W. You, *Acc. Chem. Res.*, 2017, **50**, 2401-2409.

[6] L. Nian, K. Gao, Y. Jiang, Q. Rong, X. Hu, D. Yuan, F. Liu, X. Peng, T. P. Russell and G. Zhou, *Adv. Mater.*, 2017, **29**, 1700616.

[7] J. Zhao, Y. Li, G. Yang, K. Jiang, H. Lin, H. Ade, W. Ma and H. Yan, *Nat. Energy*, 2016, **1**, 15027.

[8] S. Zhang, L. Ye and J. Hou, *Adv. Energy Mater.*, 2016, **6**, 1502529.

[9] G. Xu, L. Gao, H. Xu, L. Huang, Y. Xie, X. Cheng, Y. Li, L. Chen and Y. Chen, *J. Mater. Chem. A,* 2017, **5**, 13807-13816.

[10] W. Zhao, S. Li, H. Yao, S. Zhang, Y. Zhang, B. Yang and J. Hou, *J. Am. Chem. Soc.*, 2017, **139**, 7148-7151.

[11] Z. Fei, F. D. Eisner, X. Jiao, M. Azzouzi, J. A. Röhr, Y. Han, M. Shahid, A. S. R. Chesman, C. D. Easton, C. R. McNeill, T. D. Anthopoulos, J. Nelson and M. Heeney, *Adv. Mater.*, 2018, **30**, 1705209.

[12] W. Li, L. Ye, S. Li, H. Yao, H. Ade and J. Hou, *Adv. Mater.*, 2018, **30**, 1707170.

[13] M. A. Green, K. Emery, Y. Hishikawa, W. Warta and E. D. Dunlop, *Prog. Photovolt: Res. Appl.*, 2015, **23**, 805-812.

[14] J.-P. Correa-Baena, A. Abate, M. Saliba, W. Tress, T. Jesper Jacobsson, M. Grätzel and A. Hagfeldt, *Energy Environ. Sci.*, 2017, **10**, 710-727.

[15] D. Veldman, S. C. J. Meskers and R. A. J. Janssen, *Adv. Funct. Mater.*, 2009, **19**, 1939-1948.

[16] J. Zhang, L. Zhu and Z. Wei, *Small Methods*, 2017, **1**, 1700258.

[17] W. Li, H. Yao, H. Zhang, S. Li and J. Hou, *Chem. Asian J.*, 2017, **12**, 2160-2171.

[18] T. Linderl, T. Zechel, M. Brendel, D. Moseguí González, P. Müller-Buschbaum, J. Pflaum and W. Brütting, *Adv. Energy Mater.*, 2017, **7**, 1700237.

[19] P. K. Nayak and D. Cahen, *Adv. Mater.*, 2014, **26**, 1622-1628.

[20] J. Yao, T. Kirchartz, M. S. Vezie, M. A. Faist, W. Gong, Z. He, H. Wu, J. Troughton, T. Watson, D. Bryant and J. Nelson, *Phys. Rev. Appl.*, 2015, **4**, 014020.

[21] C. Wang, X. Xu, W. Zhang, J. Bergqvist, Y. Xia, X. Meng, K. Bini, W. Ma, A. Yartsev, K. Vandewal, M. R. Andersson, O. Inganäs, M. Fahlman and E. Wang, *Adv. Energy Mater.*, 2016, **6**, 1600148.

[22] D. Baran, T. Kirchartz, S. Wheeler, S. Dimitrov, M. Abdelsamie, J. Gorman, R. S. Ashraf, S. Holliday, A. Wadsworth, N. Gasparini, P. Kaienburg, H. Yan, A. Amassian, C. J. Brabec, J. R. Durrant and I. McCulloch, *Energy Environ. Sci.*, 2016, **9**, 3783-3793.

[23]D. Yang, H. Sasabe, T. Sano and J. Kido, *ACS Energy Lett.*, 2017, **2**, 2021-2025.

[24]J. Benduhn, K. Tvingstedt, F. Piersimoni, S. Ullbrich, Y. Fan, M. Tropiano, K. A. McGarry, O. Zeika, R M. K. iede, C. J. Douglas, S. Barlow, S. R. Marder, D. Neher, D. Spoltore and K. Vandewal, *Nat. Energy*, 2017, **2**, 17053.

[25] N. Gasparini, A. Wadsworth, M. Moser, D. Baran, I. McCulloch and C. J. Brabec, *Adv. Energy Mater.*, 2018, **8**, 1703298.

[26] P. Cheng, M. Zhang, T.-K. Lau, Y. Wu, B. Jia, J. Wang, C. Yan, M. Qin, X. Lu and X. Zhan, *Adv. Mater.*, 2017, **29**, 1605216.

[27] Z.-G. Zhang, Y. Li, L. Zhong, B. Gautam, H. Bin, J.-D. Lin, F.-P. Wu, Z. Zhang, K. Gundogdu, Y. Li, Z.-Q. Jiang and L. S. Liao, *Energy Environ. Sci.*, 2017, **10**, 1610-1620.

[28] Q. Fan, Z. Xu, X. Guo, X. Meng, W. Li, W. Su, X. Ou, W. Ma, M. Zhang and Y. Li, *Nano Energy*, 2017, **40**, 20-26.

[29] Z. Yao, X. Liao, K. Gao, F. Lin, X. Xu, X. Shi, L. Zuo, F. Liu, Y. Chen and A. K. Y. Jen, *J. Am. Chem. Soc.*, 2018, **140**, 2054-2057.

[30] W. Chen and Q. Zhang, *J. Mater. Chem. C*, 2017, **5**, 1275-1302.

[31] F. Zhao, S. Dai, Y. Wu, Q. Zhang, J. Wang, L. Jiang, Q. Ling, Z. Wei, W. Ma, W. You, C. Wang and X. Zhan, *Adv. Mater.*, 2017, **29**, 1700144.

[32] P. Cheng, G. Li, X. Zhan and Y. Yang, *Nat. Photonics*, 2018, **12**, 131-142.

[33] J. Hou, O. Inganäs, R. H. Friend and F. Gao, *Nat. Mater.*, 2018, **17**, 119-128.

[34] S. D. Collins, N. A. Ran, M. C. Heiber and T.-Q. Nguyen, *Adv. Energy Mater.*, 2017, **7**, 1602242.

[35] M. Privado, V. Cuesta, P. de la Cruz, M. L. Keshtov, G. D. Sharma and F. Langa, *J. Mater. Chem. A*, 2017, **5**, 14259-14269.

[36] N. Liang, D. Meng, Z. Ma, B. Kan, X. Meng, Z. Zheng, W. Jiang, Y. Li, X. Wan, J. Hou, W. Ma, Y. Chen and Z. Wang, *Adv. Energy Mater.*, 2017, **7**, 1601664.

[37] L. Yang, S. Zhang, C. He, J. Zhang, H. Yao, Y. Yang, Y. Zhang, W. Zhao and J. Hou, *J. Am. Chem. Soc.*, 2017, **139**, 1958-1966.

[38] H. Bin, Y. Yang, Z.-G. Zhang, L. Ye, M. Ghasemi, S. Chen, Y. Zhang, C. Zhang, C. Sun, L. Xue, C. Yang, H. Ade and Y. Li, *J. Am. Chem. Soc.*, 2017, **139**, 5085-5094.

[39] B. Qiu, L. Xue, Y. Yang, H. Bin, Y. Zhang, C. Zhang, M. Xiao, K. Park, W. Morrison, Z.-G. Zhang and Y. Li, *Chem. Mater.*, 2017, **29**, 7543-7553.

[40] L. Yang, S. Zhang, C. He, J. Zhang, Y. Yang, J. Zhu, Y. Cui, W. Zhao, H. Zhang, Y. Zhang, Z. Wei and J. Hou, *Chem. Mater.*, 2018, **30**, 2129-2134.

[41] J. Zhou, Y. Zuo, X. Wan, G. Long, Q. Zhang, W. Ni, Y. Liu, Z. Li, G. He, C. Li, B. Kan, M. Li and Y. Chen, *J. Am. Chem. Soc.*, 2013, **135**, 8484-8487.

[42] S. Holliday, R. S. Ashraf, A. Wadsworth, D. Baran, S. A. Yousaf, C. B. Nielsen, C.-H. Tan, S. D. Dimitrov, Z. Shang, N. Gasparini, M. Alamoudi, F. Laquai, C. J. Brabec, A. Salleo, J. R. Durrant and I. McCulloch, *Nat. Commun.*, 2016, **7**, 11585.

[43] J. Qi, X. Zhou, D. Yang, W. Qiao, D. Ma and Z. Y. Wang, *Adv. Funct. Mater.*, 2014, **24**, 7605-7612.

[44] M. C. Scharber, D. Mühlbacher, M. Koppe, P. Denk, C. Waldauf, A. J. Heeger and C. J. Brabec, *Adv. Mater.*, 2006, **18**, 789-794.

[45] W. Li, K. H. Hendriks, A. Furlan, M. M. Wienk and R. A. J. Janssen, *J. Am. Chem. Soc.*, 2015, **137**, 2231-2234.

[46] J. Dacuña and A. Salleo, *Phys. Rev. B*, 2011, **84**, 195209.

[47] M. Babics, R.-Z. Liang, K. Wang, F. Cruciani, Z. Kan, M. Wohlfahrt, M.-C. Tang, F.

Laquai and P. M. Beaujuge, *Chem. Mater.*, 2018, **30**, 789-798.

[48] R. Z. Liang, M. Babics, V. Savikhin, W. Zhang, V. M. L. Corre, S. Lopatin, Z. Kan, Y. Firdaus, S. Liu, I. McCulloch, M. F. Toney and P. M. Beaujuge, *Adv. Energy Mater.*, 2018, **8**, 1800264.

[49] D. Yang, Z. Guan, L. Yang, Y. Huang, Q. Wei, Z. Lu and J. Yu, Sol. *Energy Mater. Sol. Cells*, 2012, **105**, 220-228.

[50] J. Liu, S. Chen, D. Qian, B. Gautam, G. Yang, J. Zhao, J. Bergqvist, F. Zhang, W. Ma, H. Ade, O. Inganäs, K. Gundogdu, F. Gao and H. Yan, *Nat. Energy*, 2016, **1**, 16089.

Abstract Graph

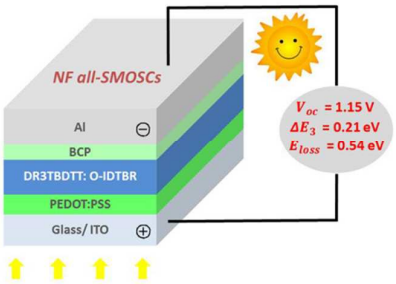

Textual Abstract

A minimal non-radiative recombination energy loss of 0.21 eV is achieved for non-fullerene all-small-molecules organic solar cells.